Int. J. Heat Mass Transfer. Vol. 34, No. 1, pp. 93–101, 1991
Printed in Great Britain

0017–9310/91 $3.00 + 0.00

Performance characteristics of a thermal energy storage module: a transient PCM/forced convection conjugate analysis

Y. CAO and A. FAGHRI
Department of Mechanical and Materials Engineering, Wright State University, Dayton, OH 45435, U.S.A.

(*Received* 28 *September* 1989 *and in final form* 15 *February* 1990)

Abstract—The performance of a thermal energy storage module is simulated numerically. The change of phase of the phase-change material (PCM) and the transient forced convective heat transfer for the transfer fluid with low Prandtl numbers are solved simultaneously as a conjugate problem. A parametric study and a system optimization are conducted. The numerical results show that module geometry is crucial to the design of a space-based thermal energy storage system.

INTRODUCTION

RECENTLY, the study of phase-change thermal energy storage systems has been active due to applications to space-based power plants and the utilization of solar energy. Phase-change materials (PCM) have a large latent heat, so it is an efficient way to absorb the heat energy during the time period when the materials are subject to heat input and to release it to space over a long period of time. A basic latent heat thermal storage geometry is shown schematically in Fig. 1. The PCM surrounds a pipe, through which the heat transfer fluid is passed. The problem by nature is a time-dependent phase-change heat transfer problem combined with conjugate forced convection.

Heat transfer involving melting and solidification is a fertile area for research because of its great importance in many applications. Since problems of this type are inherently nonlinear due to the existence of a moving interface the position of which is not known a priori, there are relatively few analytical solutions to these so-called Stefan problems. A large number of numerical techniques have been developed, but most of the numerical studies have focused on diffusion-controlled phase-change problems or phase-change problems including natural convection [1–6].

The use of a hollow cylinder of PCM similar to that in Fig. 1 for a solar latent energy storage system was modeled by Solomon *et al.* [7]. A finite difference formulation with the Kirchhoff temperature was used to calculate the internal energy, temperature, and the position of the phase-change front. Stovall and Arimilli [8] studied a thermal energy storage system consisting of a cylindrical tube filled with a phase-change material having a high melting temperature. The tube is surrounded by an annular region containing the liquid metal heat transfer fluid for pulsed power load applications. The emphasis of both of the above studies is on the diffusion-controlled heat transfer in the PCM. The heat transfer between the transfer fluid and the PCM is calculated using empirical correlations instead of solving the flow and temperature fields of the transfer fluid numerically as a conjugate problem. Also, the container wall shown in Fig. 1 was ignored. It should be pointed out that most of the empirical correlations are based on limited experimental or numerical data and the fully-developed conditions; the use of correlations may increase the uncertainty of the numerical modeling. Furthermore, the change of phase is by nature a transient problem. The boundary temperature of the transfer fluid changes as the phase-change interface progresses, therefore the temperature field of the transfer fluid may never reach the fully-developed state. This is especially important for PCM storage systems with liquid metals as the transfer fluid. With relatively shorter cylinders and lower fluid velocities, the laminar combined hydrodynamic and thermal entry region may dominate the flow along the entire length of the cylinder.

In this paper, a PCM energy storage system with the configuration in Fig. 1 is modeled numerically. The two-dimensional change of phase for the PCM and the two-dimensional transient forced convection entrance region for the transfer fluid with low Prandtl numbers is solved simultaneously. Also, the influence

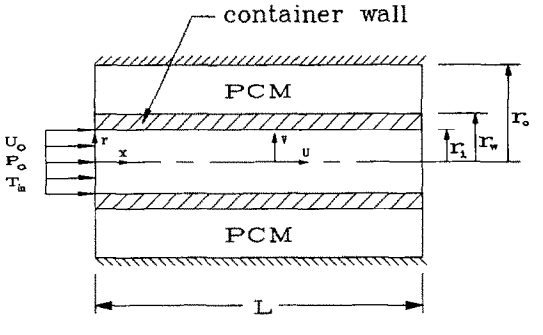

FIG. 1. The schematic of the latent heat storage system.

NOMENCLATURE

c	specific heat [J kg^{-1} K^{-1}]
c_m	specific heat of mushy phase, $1/2(c_s+c_l)$ [J kg^{-1} K^{-1}]
c_p	specific heat of PCM [J kg^{-1} K^{-1}]
C^o	coefficient in equation (5) [J kg^{-1} K^{-1}]
C	C^o/c_l
C_{sl}	c_s/c_l
D	inside diameter of the circular pipe, or diagonal distance [m]
g_l	integral in equation (18)
g_t	integral in equation (19)
H	latent heat [J kg^{-1}]
k	thermal conductivity [W m^{-1} K^{-1}]
K	dimensionless thermal conductivity, k/k_l
K_{sl}	k_s/k_l
L	length of pipe [m] reference length in Fig. 2 [m]
m	total mass of the PCM [kg]
p	pressure [N m^{-2}]
p_o	inlet pressure [N m^{-2}]
P	dimensionless pressure, $(p-p_o)/\rho_f U_o^2$
Pr_f	fluid Prandtl number, ν_f/α_f
Q	heat energy [J]
Q_l	total latent energy stored [J]
Q_t	total energy stored [J]
Q_m	energy storage density [J kg^{-1}]
Re_f	fluid Reynolds number, $U_o D/\nu_f$
S^o	term in equation (5) [J kg^{-1}]
S	$S^o/c_l(T_{in}^o-T_m^o)$
s	interface position along the diagonal [m]
St	Stefan number, $c_l(T_{in}^o-T_m^o)/H$
T^o	temperature [K]
T_m^o	melting temperature [K]
T	dimensionless temperature, $(T^o-T_m^o)/(T_{in}^o-T_m^o)$
T^*	scaled temperature, $T^o-T_m^o$ [K]
t	time [s]
U_o	inlet velocity [m s^{-1}]
U, V	dimensionless velocities, u/U_o, v/U_o
u, v	velocities [m s^{-1}]
X, R	dimensionless coordinate directions, x/D, r/D
x, r	coordinate directions.

Greek symbols

α	thermal diffusivity [m^2 s^{-1}]
$2\delta T^o$	phase-change temperature range, or mushy phase range [6] [K]
δT^*	$\delta T^o/(T_{in}^o-T_m^o)$
ν	kinematic viscosity [m^2 s^{-1}]
ρ	density [kg m^{-3}]
τ	dimensionless time, $U_o t/D$.

Subscripts

f	transfer fluid
i	initial condition, or inside radius of the pipe
in	inlet
inf	melting interface
l	liquid PCM or latent heat
m	mass or mushy phase
o	outer surface of the PCM module
p	PCM
s	solid PCM
w	container wall.

of the container wall is included in the numerical analysis, and an optimization of the configuration is conducted. To the authors' knowledge, this work is the first PCM/forced convection conjugate problem reported in the literature.

MATHEMATICAL MODELING

The continuity, momentum, and energy equations governing two-dimensional transient incompressible laminar flows with no viscous dissipation in a pipe are [9]

$$\frac{1}{r}\frac{\partial}{\partial r}(rv)+\frac{\partial u}{\partial x}=0 \tag{1}$$

$$\frac{\partial v}{\partial t}+v\frac{\partial v}{\partial r}+u\frac{\partial v}{\partial x}=-\frac{1}{\rho_f}\frac{\partial p}{\partial r}+\nu_f\left[\frac{1}{r}\frac{\partial}{\partial r}\left(r\frac{\partial v}{\partial r}\right)-\frac{v}{r^2}+\frac{\partial^2 v}{\partial x^2}\right] \tag{2}$$

$$\frac{\partial u}{\partial t}+v\frac{\partial u}{\partial r}+u\frac{\partial u}{\partial x}=-\frac{1}{\rho_f}\frac{\partial p}{\partial x}+\nu_f\left[\frac{1}{r}\frac{\partial}{\partial r}\left(r\frac{\partial u}{\partial r}\right)+\frac{\partial^2 u}{\partial x^2}\right] \tag{3}$$

$$\rho_f c_f\left(\frac{\partial T^o}{\partial t}+v\frac{\partial T^o}{\partial r}+u\frac{\partial T^o}{\partial x}\right)=k_f\left[\frac{1}{r}\frac{\partial}{\partial r}\left(r\frac{\partial T^o}{\partial r}\right)+\frac{\partial^2 T^o}{\partial x^2}\right]. \tag{4}$$

For the PCM, the temperature transforming model [6] is used. The energy equation is written as

$$\frac{\partial(\rho C^o T^*)}{\partial t}=\frac{1}{r}\frac{\partial}{\partial r}\left(kr\frac{\partial T^*}{\partial r}\right)+\frac{\partial}{\partial x}\left(k\frac{\partial T^*}{\partial x}\right)-\frac{\partial(\rho S^o)}{\partial t} \tag{5}$$

where $T^*=T^o-T_m^o$

$$C^\circ = C^\circ(T^*) = \begin{cases} c_s & (T^* < -\delta T^\circ) \quad \text{(solid phase)} \\ c_m + \dfrac{H}{2\delta T^\circ} & (-\delta T^\circ \leqslant T^* \leqslant \delta T^\circ) \quad \text{(mushy phase)} \\ c_l & (T^* > \delta T^\circ) \quad \text{(liquid phase)} \end{cases} \tag{6}$$

$$S^\circ = S^\circ(T^*) = \begin{cases} c_s \delta T^\circ & (T^* < -\delta T^\circ) \quad \text{(solid phase)} \\ c_m \delta T^\circ + \dfrac{H}{2} & (-\delta T^\circ \leqslant T^* \leqslant \delta T^\circ) \quad \text{(mushy phase)} \\ c_s \delta T^\circ + H & (T^* > \delta T^\circ) \quad \text{(liquid phase)} \end{cases} \tag{7}$$

$$k(T^*) = \begin{cases} k_s & (T^* < -\delta T^\circ) \quad \text{(solid phase)} \\ k_s + (k_l - k_s)(T^* + \delta T^\circ)/2\delta T^\circ & (-\delta T^\circ \leqslant T^* \leqslant \delta T^\circ) \quad \text{(mushy phase)} \\ k_l & (T^* > \delta T^\circ) \quad \text{(liquid phase).} \end{cases} \tag{8}$$

For the pipe wall, the energy equation is

$$\rho_w c_w \frac{\partial T^\circ}{\partial t} = k_w \left[\frac{1}{r} \frac{\partial}{\partial r} \left(r \frac{\partial T^\circ}{\partial r} \right) + \frac{\partial^2 T^\circ}{\partial x^2} \right]. \tag{9}$$

The initial and boundary conditions for the case of uniform inlet conditions are defined as follows:

initial conditions: $t = 0$

entire domain: $0 \leqslant x \leqslant L$, $0 < r < r_o$

$$T^\circ = T_i^\circ, \quad u = v = 0$$

boundary conditions: $t > 0$

inlet plane: $x = 0$

$$0 < r < r_i: \quad u = U_o, \quad T^\circ = T_{in}^\circ, \quad v = 0$$

$$r_i < r < r_o: \quad \frac{\partial T^\circ}{\partial x} = 0$$

outer wall: $0 < x < L$, $r = r_o$

$$\left. \frac{\partial T^\circ}{\partial r} \right|_{r = r_o} = 0$$

PCM–wall interface: $0 < x < L$, $r = r_w$

$$k_p \left. \frac{\partial T^\circ}{\partial r} \right|_{r = r_w^+} = k_w \left. \frac{\partial T^\circ}{\partial r} \right|_{r = r_w^-}$$

wall–fluid interface: $0 < x < L$, $r = r_i$

$$k_w \left. \frac{\partial T^\circ}{\partial r} \right|_{r = r_i^+} = k_f \left. \frac{\partial T^\circ}{\partial r} \right|_{r = r_i^-}$$

outlet plane: $x = L$

$$0 < r < r_o: \quad \frac{\partial T^\circ}{\partial x} = 0$$

$$0 < r < r_i: \quad \frac{\partial u}{\partial x} = 0.$$

The use of the temperature transforming model [6] has two advantages. First, equations (5)–(8) form a set of closed-group equations, so an explicit treatment of the phase-change interface is not needed. Secondly, the time step and grid size limitations are eliminated, which are normally encountered for other fixed-grid methods. It should be pointed out that due to the space application the natural convection in the liquid PCM has been ignored.

The following non-dimensional variables are introduced:

$$R = r/D, \quad X = \frac{x}{D}, \quad U = \frac{u}{U_o}, \quad V = \frac{v}{U_o}, \quad Re_f = \frac{U_o D}{\nu_f},$$

$$T = \frac{T^\circ - T_m^\circ}{T_{in}^\circ - T_m^\circ}, \quad \tau = \frac{U_o}{D} t, \quad P = \frac{p - p_o}{\rho_f U_o^2},$$

$$C = \frac{C^\circ}{c_l}, \quad K = \frac{k}{k_l}, \quad S = S^\circ / c_l (T_{in}^\circ - T_m^\circ),$$

$$St = c_l (T_{in}^\circ - T_m^\circ)/H, \quad \delta T^* = \delta T^\circ / (T_{in}^\circ - T_m^\circ).$$

The dimensionless continuity, momentum and energy equations for the transfer fluid are as follows:

$$\frac{1}{R} \frac{\partial}{\partial R}(RV) + \frac{\partial U}{\partial X} = 0 \tag{10}$$

$$\frac{\partial U}{\partial \tau} + V \frac{\partial U}{\partial R} + U \frac{\partial U}{\partial X} = -\frac{\partial P}{\partial X} + \frac{1}{Re_f} \left[\frac{1}{R} \frac{\partial}{\partial R} \left(R \frac{\partial U}{\partial R} \right) + \frac{\partial^2 U}{\partial X^2} \right] \tag{11}$$

$$\frac{\partial V}{\partial \tau} + V \frac{\partial V}{\partial R} + U \frac{\partial V}{\partial X} = -\frac{\partial P}{\partial R} + \frac{1}{Re_f} \left[\frac{1}{R} \frac{\partial}{\partial R} \left(R \frac{\partial V}{\partial R} \right) + \frac{\partial^2 V}{\partial X^2} - \frac{V}{R^2} \right] \tag{12}$$

$$\frac{\partial T}{\partial \tau} + V \frac{\partial T}{\partial R} + U \frac{\partial T}{\partial X} = -\frac{\partial P}{\partial R} + \frac{1}{Re_f Pr_f} \left[\frac{1}{R} \frac{\partial}{\partial R} \left(R \frac{\partial T}{\partial R} \right) + \frac{\partial^2 T}{\partial X^2} \right]. \tag{13}$$

The dimensionless energy equation for the PCM is

$$\frac{\partial (CT)}{\partial \tau} = \frac{1}{Re_f Pr_f} \frac{\alpha_l}{\alpha_f} \left[\frac{1}{R} \frac{\partial}{\partial R} \left(KR \frac{\partial T}{\partial R} \right) + \frac{\partial}{\partial X} \left(K \frac{\partial T}{\partial X} \right) \right] - \frac{\partial S}{\partial \tau} \tag{14}$$

where

$$C(T) = \begin{cases} C_{sl} & (T < -\delta T^*) \\ \frac{1}{2}(1+C_{sl}) + \dfrac{1}{2St\,\delta T^*} & (-\delta T^* \leqslant T \leqslant \delta T^*) \\ 1 & (T > \delta T^*) \end{cases}$$

$$S(T) = \begin{cases} C_{sl}\delta T^* & (T < -\delta T^*) \\ \frac{1}{2}\delta T^*(1+C_{sl}) + \dfrac{1}{2St} & (-\delta T^* \leqslant T \leqslant \delta T^*) \\ C_{sl}\delta T^* + \dfrac{1}{St} & (T > \delta T^*) \end{cases}$$

$$K(T) = \begin{cases} K_{sl} & (T < -\delta T^*) \\ K_{sl} + (1-K_{sl})(T+\delta T^*)/2\delta T^* & (-\delta T^* \leqslant T \leqslant \delta T^*) \\ 1 & (T > \delta T^*). \end{cases}$$

The dimensionless energy equation for the container wall is

$$\frac{\partial T}{\partial \tau} = \frac{1}{Re_f\, Pr_f} \frac{\alpha_w}{\alpha_f} \left[\frac{1}{R} \frac{\partial}{\partial R} \left(R \frac{\partial T}{\partial R} \right) + \frac{\partial^2 T}{\partial X^2} \right]. \quad (15)$$

The initial and boundary conditions are non-dimensionalized as follows:

initial conditions: $\tau = 0$

entire domain: $0 \leqslant X \leqslant L/D$, $0 \leqslant R \leqslant R_o$

$$T = T_i, \quad U = V = 0 \quad (16a)$$

boundary conditions: $\tau > 0$

inlet plane: $X = 0$

$$0 < R < 0.5: \quad U = 1, T = 1, V = 0$$

$$0.5 < R < R_o: \quad \frac{\partial T}{\partial X} = 0 \quad (16b)$$

outer wall: $0 < X < L/D$, $R = R_o$

$$\left. \frac{\partial T}{\partial R} \right|_{R = R_o} = 0 \quad (16c)$$

PCM–wall interface: $0 < X < L/D$, $R = R_w$

$$\frac{k_p}{k_w} \left. \frac{\partial T}{\partial R} \right|_{R = R_w^+} = \left. \frac{\partial T}{\partial R} \right|_{R = R_w} \quad (16d)$$

wall–fluid interface: $0 < X < L/D$, $R = 0.5$

$$\left. \frac{\partial T}{\partial R} \right|_{R = 0.5^+} = \frac{k_f}{k_w} \left. \frac{\partial T}{\partial R} \right|_{R = 0.5} \quad (16e)$$

outer plane: $X = L/D$

$$0 < R < R_o: \quad \frac{\partial T}{\partial X} = 0$$

$$0 < R < 0.5: \quad \frac{\partial U}{\partial X} = 0. \quad (16f)$$

It can be seen that the temperature field can be expressed as

$$T = T(\tau, R, X, Re_f, Pr_f, \alpha_l/\alpha_f, \alpha_w/\alpha_f, St, C_{sl}, \delta T^*, K_{sl}, k_f/k_w, k_p/k_w, r_w/D, r_o/D, L/D). \quad (17)$$

NUMERICAL PROCEDURE

The problem has been specified mathematically by equations (10)–(16). The solution procedure used for solving these equations is the control-volume finite-difference approach described by Patankar [10, 11]. In this methodology, the discretization equations are obtained by applying the conservation laws over a finite size control volume surrounding the grid node and integrating the equation over the control volume. The velocities and pressure are solved by using the SIMPLE scheme [10]. At the PCM–wall and the wall–fluid interfaces, the harmonic mean of the thermal conductivity with a uniform grid size is

$$k_p \left. \frac{\partial T^o}{\partial r} \right|_{r = r_w^-} = k_w \left. \frac{\partial T^o}{\partial r} \right|_{r = r_w^-} = \frac{2k_p k_w}{k_p + k_w} \left. \frac{\partial T^o}{\partial r} \right|_{r = r_w}$$

$$k_w \left. \frac{\partial T^o}{\partial r} \right|_{r = r_i^+} = k_f \left. \frac{\partial T^o}{\partial r} \right|_{r = r_i^-} = \frac{2k_w k_f}{k_w + k_f} \left. \frac{\partial T^o}{\partial r} \right|_{r = r_i}.$$

The discretization equations are solved by using the tridiagonal matrix algorithm (TDMA or Thomas algorithm). During each time step, iterations are needed. The converged results were assumed to be reached when the maximum relative change of all variables between consecutive iterations was less than 0.1%. The residual of the continuity equation was also checked. The iteration was continued until the sum of the residuals was less than 10^{-5}. Different grid sizes for the same problem have been tested and it proves that both the PCM model and the numerical scheme used for the transfer fluid are essentially independent of grid sizes for the numerical results in the next section. The space and time grid specifications are given in the next section for the cases presented.

NUMERICAL RESULTS AND DISCUSSION

Before presenting the numerical results for the phase-change system, the phase-change model (equation (5)) was checked against other numerical results for a two-dimensional freezing problem. Consider a liquid initially at T_i^o in an infinitely long prism with a uniform cross section [12]. At $t > 0$, the surface is kept at a temperature $T_w^o < T_m^o$ and freezing takes place immediately. Because of the symmetry of the

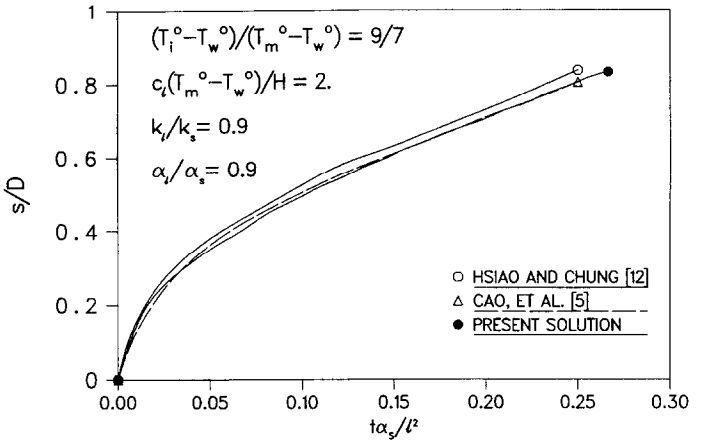

FIG. 2. Interface position along the diagonal with prescribed boundary temperature.

geometry, only a quarter of the prism is considered. Figure 2 shows the interface position as a function of $t\alpha_s/l^2$ along the diagonal. Also included in this figure are solutions by Hsiao and Chung [12], and by Cao *et al.* [5]. It can be seen that the present model agrees well with the results of these studies.

The numerical calculations for the thermal energy storage system were then conducted with the configuration as shown in Fig. 1. The system is initially at a temperature $T_i < 0$ (less than the melting temperature of the PCM). The hotter fluid enters into the circular channel and heats the system, which absorbs the energy from the fluid and stores it as both latent and sensible heat. The grid size used for the calculations was 70 (axial) × 20 (radial transfer fluid) × 5 (container wall) × 15 (PCM) with dimensionless time steps of $\Delta\tau = 5$ or 10. In order to simulate the phase change at a single temperature using equation (14), the dimensionless phase-change temperature δT^* is taken to be 0.01.

Figure 3 shows the axial velocity distribution in the radial direction at $X = 6$ at different times. It can be seen that the velocity reaches the steady state quickly. After $\tau = 20$, the velocity profile remains unchanged. This does not mean the velocity profile has reached the fully developed condition along the pipe. Since the pipe is comparatively short and the Prandtl number is small, the developing velocity region is dominant along the whole pipe length. The temperature profile, however, is different. Figure 4 shows the radial temperature distribution at $X = 6$ for different time periods. The three regions in the radial direction (transfer fluid, container wall, and the PCM) are also indicated in the figure. The melting interfaces at different times are the intersections of $T = 0$ and the corresponding temperature curves. It can be seen that as the melting interface progresses, the temperature curve moves upward accordingly. Although the velocity field of the transfer fluid reaches the steady state quickly, its temperature counterpart cannot reach the steady state before the PCM is totally melted. This clearly demonstrates that the use of steady fully-developed empirical heat transfer correlations for the transfer fluid may result in a significant error for the evaluation of the system performance.

Figure 5 shows the melting interface along the axial direction at different times. At $\tau = 1000$, the melting interface has reached the outer surface ($r = r_o$) for $X < 6$, while some PCM remains unmelted for $X > 6$. The reason is that since the Prandtl number of the transfer fluid is very small (the thermal conductivity is very large) a large amount of heat is transferred directly to the PCM upstream while a relatively small amount of heat is carried downstream. Figure 6 shows the melting interfaces along the axial direction for the transfer fluids with different Prandtl numbers. With a smaller Prandtl number, heat transfer to the PCM is much faster as indicated in the figure.

As in normal forced convective heat transfer, the Reynolds number has a significant influence on the system performance. This is illustrated in Fig. 7 with the same Prandtl number and different Reynolds numbers. Since the dimensionless time τ contains the inlet velocity U_o, the comparison has been made at a dimensional time t. The dimensionless time for the case of $Re_f = 2200$ was taken as $\tau = 1000$, the corresponding dimensionless times for $Re_f = 1700$ and 1200 were 773 and 545, respectively, with the assumption of the same D and ν_f for the three cases.

Since the transfer fluid is a liquid metal, the thermal conductivity has the same order of magnitude as that of the container wall. The influence of the thermal conductivity of the wall on the system performance may not be as important as those using gases as transfer fluids, as illustrated in Fig. 8.

It is very important to evaluate the overall performance of the system and to optimize the geometry of the system with given flow parameters and thermal properties. The important system parameters used to evaluate a thermal energy storage system are the energy storage capacity or total energy stored Q_t (J), the energy storage density $Q_m = Q_t/m$ (J kg^{-1}), the

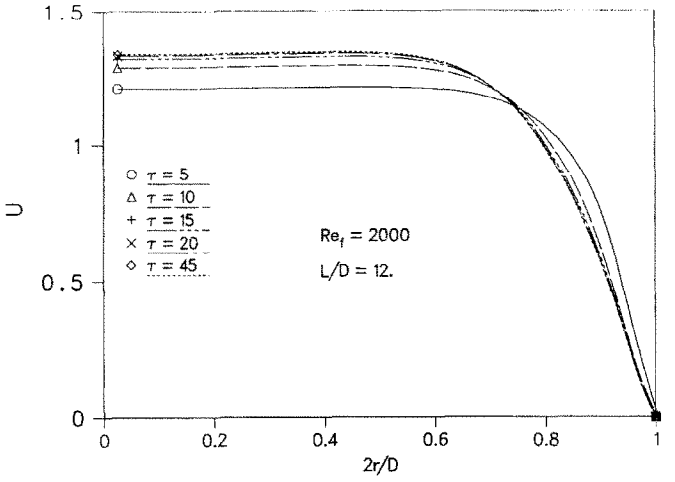

FIG. 3. Axial velocity distribution of transfer fluid at $X = 6$ for different time periods.

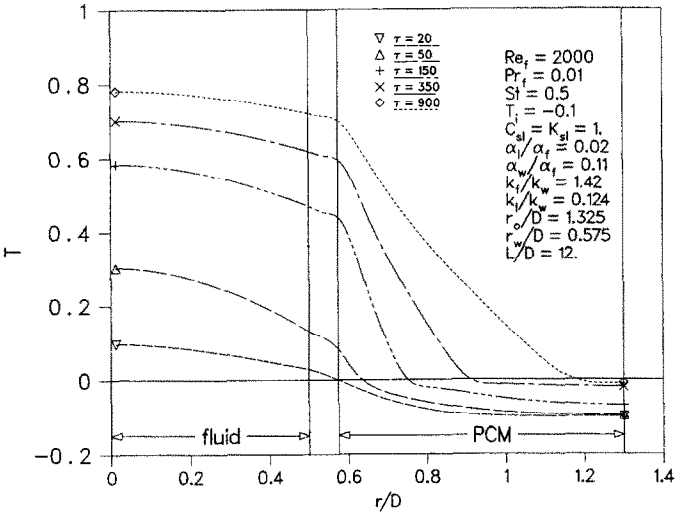

FIG. 4. Radial temperature distribution at $X = 6$ for different time periods.

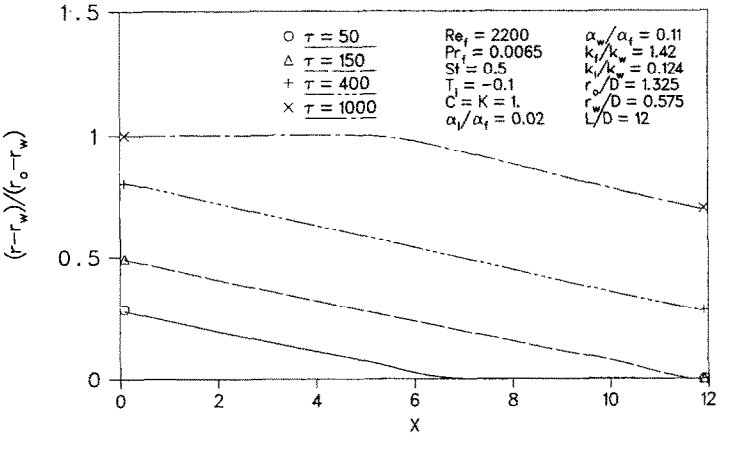

FIG. 5. Melting fronts along the axial direction for different time periods.

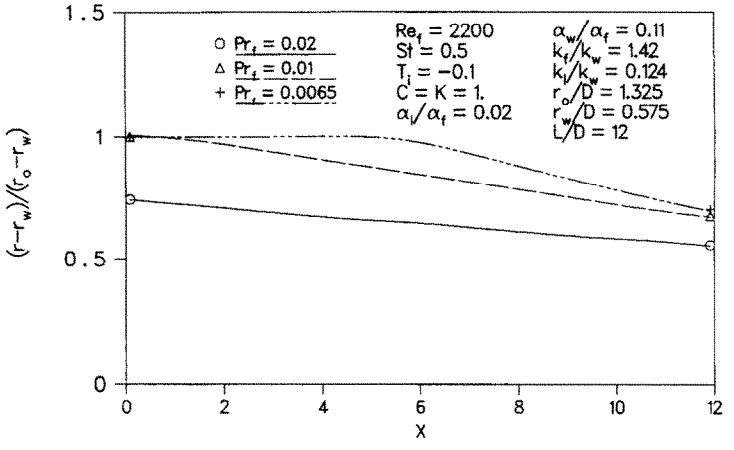

FIG. 6. Melting fronts along the axial direction for different Prandtl numbers at $\tau = 1000$.

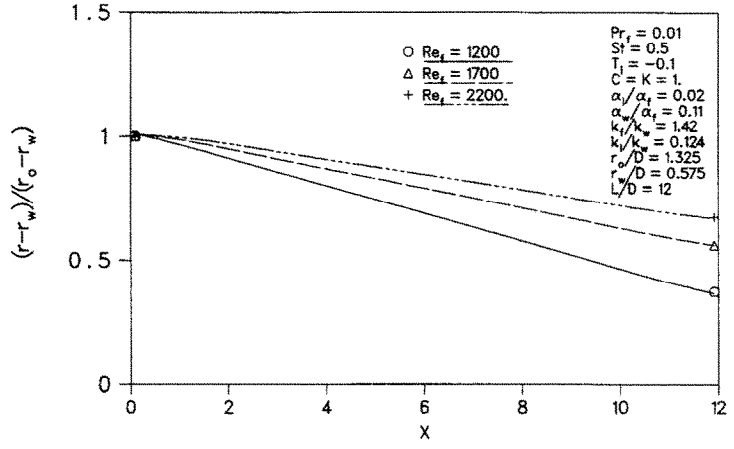

FIG. 7. Melting fronts along the axial direction for different Reynolds numbers.

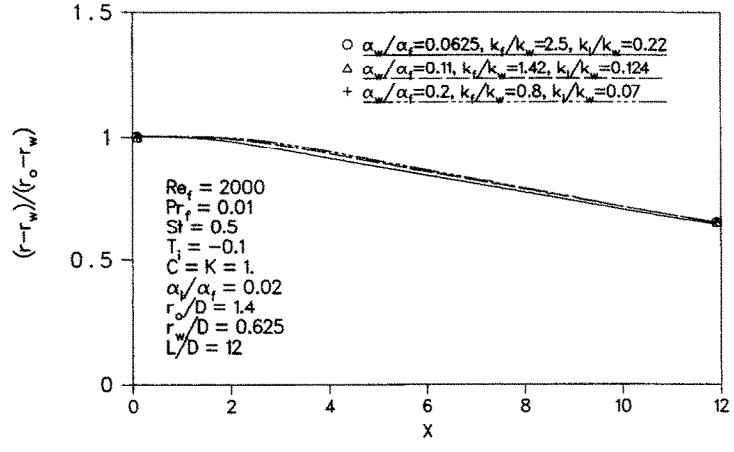

FIG. 8. Melting fronts along the axial direction for different thermal conductivities of the wall at $\tau = 1000$.

total latent energy stored Q_l (J) and the ratio of the latent to the total energy stored Q_l/Q_t. The first two parameters, Q_t and Q_m, are most important to an energy storage system. In many cases, the energy storage capacity is the primary parameter one would be concerned with, while for a space application the energy storage density is equally important because the weight of the system is critical. With reference to the geometry shown in Fig. 1, they can be expressed as

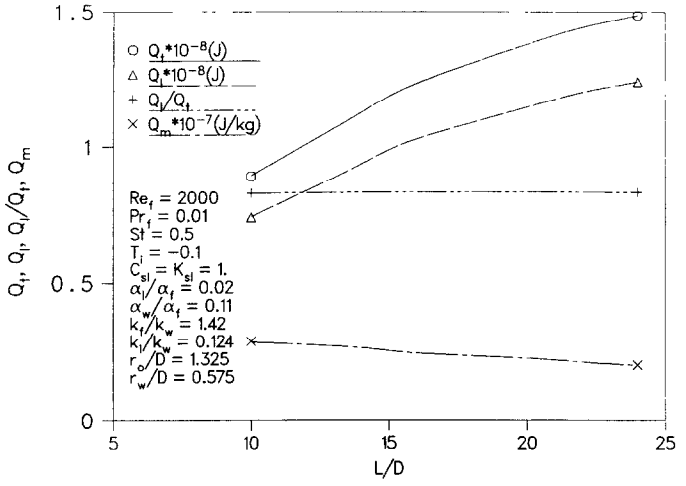

FIG. 9. System optimization analysis for different L/D at $\tau = 1000$.

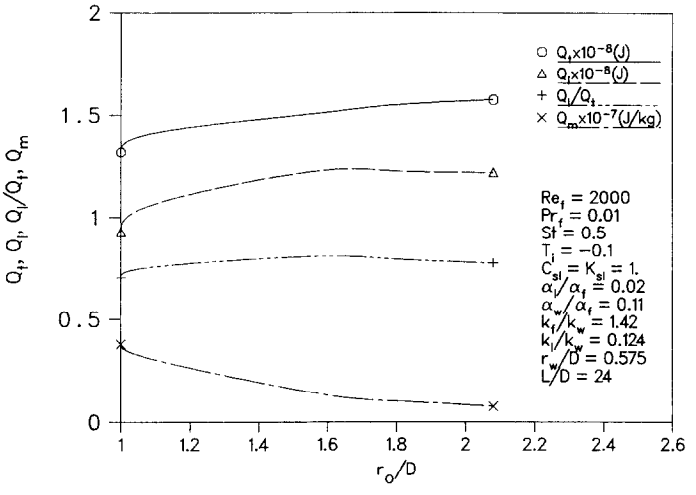

FIG. 10. System optimization analysis for different r_o/D at $\tau = 1000$.

$$Q_l = D^3\rho_p H\pi \int_0^{L/D} (R_{inf}^2(X) - R_w^2)\,dX = D^3\rho_p H\pi g_l \tag{18}$$

where $R_{inf}(X)$ is the radial location of the melting interface along the x-direction, and

$$g_l = \int_0^{L/D} (R_{inf}^2(X) - R_w^2)\,dX$$

$$Q_t = Q_l + 2\pi D^3 c_p\rho_p(T_{in}^o - T_m^o) \times \int_{R_w}^{R_o}\int_0^{L/D} (T - T_i)R\,dR\,dX = Q_l + 2\pi D^3 c_p\rho_p(T_{in}^o - T_m^o)g_t \tag{19}$$

where

$$g_t = \int_{R_w}^{R_o}\int_0^{L/D} (T - T_i)R\,dR\,dX$$

$$Q_t/Q_l = 1 + 2St\,g_t/g_l \tag{20}$$

$$Q_m = Q_t/m = Hg_l/(R_o^2 - R_w^2)\frac{L}{D} + 2(T_{in}^o - T_m^o)c_p g_t/(R_o^2 - R_w^2)\frac{L}{D}. \tag{21}$$

Figures 9 and 10 present the numerical results for the system optimization analysis for different L/D and r_o/D. The dimensional parameters needed in equations (18)–(21) are $H = 2.9 \times 10^6$ J kg^{-1}, $\rho_p = 690$ kg m^{-3}, $c_p = 7420$ J kg^{-1} K^{-1}, $T_{in}^o - T_m^o = 195.4$ K and $D = 0.1$ m. Both Q_t and Q_l follow the trend of increasing with larger L/D and r_o/D, while Q_l/Q_t remains almost constant. The high proportion of latent heat storage in the PCM is largely attributable to the small difference between the initial system temperature and PCM melt temperature ($T_i = -0.1$). The trend of the energy storage density is different from those of Q_t

and Q_l. The energy storage density Q_m drops slightly with the increase in L/D because the increase of Q_l balances in part that of the total mass m which increases with L/D. On the other hand, Q_m drops significantly with the increase in r_o/D. In this situation, a trade-off needs to be reached when selecting the design parameters.

CONCLUSIONS

An energy storage system with the configuration in Fig. 1 has been studied numerically. Numerical results show that the fluid velocity inside the pipe reaches the steady state quickly, while the temperature field continues to change as the melting interface progresses. It is very important to treat the phase change and the fluid flow as a conjugate problem and solve them simultaneously. The numerical results for the parametric study and geometry optimization provide guidelines for the design of a space-based thermal energy storage system.

Acknowledgement—Funding for the work was provided by a joint effort of the NASA Lewis Research Center and the Thermal Energy Group of the Aero Propulsion Laboratory of the U.S. Air Force under contract F33615-89-C-2820.

REFERENCES

1. N. Shamsundar and E. M. Sparrow, Analysis of multidimensional conduction phase change via the enthalpy model, *J. Heat Transfer* **97**(3), 333–340 (1975).
2. V. R. Voller and M. Cross, Estimating the solidification/melting times of cylindrically symmetric regions, *Int. J. Heat Mass Transfer* **24**, 1457–1461 (1981).
3. E. M. Sparrow and Y. Ohkuho, Numerical analysis of two-dimensional transient freezing including solid-phase and tube-wall conduction and liquid-phase natural convection, *Numer. Heat Transfer* **9**, 59–77 (1986).
4. V. R. Voller and C. Prakash, A fixed grid numerical modelling methodology for convection–diffusion mushy region phase-change problems, *Int. J. Heat Mass Transfer* **30**, 1709–1718 (1987).
5. Y. Cao, A. Faghri and W. S. Chang, A numerical analysis of Stefan problems for generalized multi-dimensional phase-change structures using the enthalpy transforming model, *Int. J. Heat Mass Transfer* **32**, 1289–1298 (1989).
6. Y. Cao and A. Faghri, A temperature transforming model with a fixed grid numerical methodology for phase-change problems including natural convection, *ASME J. Heat Transfer* **112**(3), 812–816 (1990).
7. A. D. Solomon, M. D. Morris, J. Martin and M. Olszewski, The development of a simulation code for a latent heat thermal energy storage system in a space station, Technical Report ORNL-6213 (1986).
8. T. K. Stovall and R. V. Arimilli, Transient thermal analysis of three fast-changing latent heat storage configuration for a space-based power system, *Proc. 23rd Intersociety Energy Conversion Engng Conf.*, pp. 171–177 (1988).
9. E. N. Ganic, J. P. Hartnett and W. M. Rohsenow, Basic concepts of heat transfer. In *Handbook of Heat Transfer Fundamentals* (Edited by W. M. Rohsenow *et al.*), pp. 15–25 (1985).
10. S. V. Patankar, *Numerical Heat Transfer and Fluid Flow*. McGraw-Hill, New York (1980).
11. S. V. Patankar, Elliptic systems: finite-difference method I. In *Handbook of Numerical Heat Transfer* (Edited by W. J. Minkowycz *et al.*), pp. 215–290 (1988).
12. J. S. Hsiao and B. T. F. Chung, An efficient algorithm for finite element solution to two-dimensional heat transfer with melting and freezing, ASME Paper No. 84-HT-2 (1984).

CARACTERISTIQUES DE PERFORMANCE D'UN MODULE DE STOCKAGE D'ENERGIE THERMIQUE: ANALYSE D'UNE CONJUGAISON PCM/CONVECTION FORCEE VARIABLE

Résumé—On simule numériquement la performance d'un module de stockage d'énergie thermique. On résout simultanément comme un problème conjugué le changement de phase du matériau (PCM) et le transfert par convection forcée variable d'un fluide à faible nombre de Prandtl. Une étude paramétrique est faite avec une optimisation. Les résultats numériques montrent que la géométrie du module est cruciale pour la conception d'un système de stockage d'énergie thermique.

DAS CHARAKTERISTISCHE VERHALTEN EINES WÄRMESPEICHERS—UNTERSUCHUNG DES KONJUGIERTEN PROBLEMS AUS INSTATIONÄREM PHASENWECHSEL UND ERZWUNGENER KONVEKTION

Zusammenfassung—Das Verhalten eines Wärmespeichers wird numerisch simuliert. Dabei wird der Phasenwechsel und die instationäre erzwungene Konvektion bei kleiner Prandtl-Zahl simultan als konjugiertes Problem berechnet. Eine Parameter-Untersuchung und eine Systemoptimierung werden durchgeführt. Die numerischen Ergebnisse zeigen, daß die Speichergeometrie ausschlaggebend für die Konstruktion des gesamten Speichersystems für Raumfahrtanwendungen ist.

РАБОЧИЕ ХАРАКТЕРИСТИКИ МОДУЛЯ НАКОПЛЕНИЯ ТЕПЛОВОЙ ЭНЕРГИИ: СОВМЕСТНЫЙ АНАЛИЗ НЕСТАЦИОНАРНОГО ФАЗОВОГО ПЕРЕХОДА И ВЫНУЖДЕННОЙ КОНВЕКЦИИ

Аннотация—Численно моделируются рабочие характеристики модуля накопления тепловой энергии. Фазовый переход в материале и теплоперенос за счет нестационарной вынужденной конвекции при течении жидкости с низкими числами Прандтля исследуется совместно как сопряженная задача. Проводятся параметрический анализ и оптимизация системы. Численные результаты показывают, что геометрия модуля является решающим фактором при разработке тепловых энергетических систем для космических аппаратов.